AGU PUBLICATIONS

JGR

Journal of Geophysical Research: Space Physics

RESEARCH ARTICLE
10.1002/2015JA021320

Key Points:
- Daytime E region irregularity structure is examined using VHF scintillation
- Small-scale irregularities are more likely on counter equatorial electrojet (CEEJ) days than non-CEEJ days
- Theoretical model suggests presence of 6–19% density fluctuations in *E* region

Correspondence to:
V. Yadav,
virendray.iig@gmail.com

Citation:
Yadav, V., B. Kakad, T. K. Pant, A. Bhattacharyya, and D. S. V. V. D. Prasad (2015), Study of equatorial *E* region irregularities using rare daytime VHF scintillation observations, *J. Geophys. Res. Space Physics*, *120*, doi:10.1002/2015JA021320.

Received 10 APR 2015
Accepted 23 SEP 2015
Accepted article online 28 SEP 2015

Study of equatorial *E* region irregularities using rare daytime VHF scintillation observations

V. Yadav[1], B. Kakad[1], T. K. Pant[2], A. Bhattacharyya[1], and D. S. V. V. D. Prasad[3]

[1]Indian Institute of Geomagnetism, Navi Mumbai, India, [2]Space Physics Laboratory, Vikram Sarabhai Space Centre, Trivandrum, India, [3]Department of Physics, Andhra University, Visakhapatnam, India

Abstract Scintillations on VHF radio signal are sparsely observed during daytime due to unavailability of strong electron density irregularities in equatorial *E* or *F* region. Type I/II irregularities observed at *E* region altitudes during the daytime are linked with either two-stream or gradient drift instability. The occurrence of these irregularities in presence of strong blanketing E_s (E_{sb}) can produce weak-moderate scintillations on VHF signal during daytime. Such sparse daytime VHF scintillations are used in the present study to retrieve information about *E* region irregularities, which are generally examined with radar observations. We use spaced receiver scintillation observations on 251 MHz signal transmitted from geostationary satellite UFO2 (71.2°E) and recorded at Tirunelveli (8.5°N, 77.8°E, dip latitude 0.6°N). Ionosonde data from Trivandrum (8.5°N, 76.6°E, dip latitude 0.5°N) during 2003–2005 is used to confirm the association of daytime scintillations with E_{sb}. The daytime scintillations last for 15–45 min during postnoon hours. Their occurrence closely matches the peak occurrence time of E_{sb}. For the first time, spatial scale lengths of *E* region irregularities are obtained using the technique introduced by Bhattacharyya et al. (2003). The observed spatial scales are validated using theoretical model. The theoretical model manifests 6–19% density fluctuations in the *E* region to produce weak scintillations ($0.15 \leq S_4 \leq 0.4$) on 251 MHz. The study reveals that scale lengths of *E* region irregularities are smaller on counter equatorial electrojet (CEEJ) days than non-CEEJ days, which could be resulting from lower electron temperatures in *E* region on CEEJ days.

1. Introduction

Equatorial *E* region irregularities are of particular interest due to their close association with equatorial electrojet (EEJ) current system. Two different types of irregularities are generally observed in the equatorial *E* region, namely, Types I and II. Type I irregularities are generated by modified two-stream instability mechanism, when the electron drift velocity with respect to the ions exceeds the ion acoustic velocity [*Farley Jr.*, 1963; *Buneman*, 1963], whereas Type II irregularities are produced by gradient drift instability mechanism in the presence of vertical electron density gradient parallel to the vertical polarization electric field that drives the electrojet current [*Schmidt and Peter Gary*, 1973; *Farley and Fejer*, 1975; *Devasia et al.*, 2004, and references therein]. The signatures of these irregularities are also frequently seen in the ionosonde observations as sporadic *E* (E_s) [*Anastassiadis and Matsoukas*, 1970; *Dasgupta and Kersley*, 1976]. In earlier studies, these irregularities have been examined mostly using radar observations at low [*Farley and Balsley*, 1973; *Fejer et al.*, 1975; *Reddy and Devasia*, 1977] and midlatitude or high latitudes [*Ecklund et al.*, 1981; *Hanuise*, 1983]. However, through radar, one can study only a particular scale size that is of the order of $\sim \lambda/2$, where λ is the radar wavelength. Here we use sparse daytime VHF scintillations to investigate the structuring of *E* region irregularities on quiet days in presence/absence of counter electrojet (CEEJ).

In postsunset hours, equatorial spread *F* (ESF) irregularities are strong enough to produce amplitude and phase scintillations on incoming VHF/GHz radio signal. Such observations are used globally to study ESF irregularities [*Wernik et al.*, 1983; *Bhattacharyya et al.*, 1989, 2001; *Valladares et al.*, 1996; *Ledvina et al.*, 2004; *Kakad et al.*, 2007, 2012]. Daytime scintillations on VHF signal are observed less frequently due to the unavailability of strong electron density irregularities in the equatorial *E* or *F* region. An interesting phenomenon observed at *E* region altitude is blanketing sporadic *E* (E_{sb}), which is a thin layer of highly dense ionization that blocks the upper ionospheric layers to ionosonde radio waves. The occurrence of Type I/II irregularities, in presence of E_{sb}, can cause weak-moderate scintillations even on VHF signals during daytime. Such daytime VHF scintillations have been studied in past using single receiver observations [*Basu et al.*, 1977; *Rastogi and Mullen*, 1981;

Bhattacharyya and Rastogi, 1986; *Bhattacharyya*, 1991]. However, the structuring or spatial scale lengths of *E* region irregularities producing these scintillations were not explored. The advantage of spaced receiver scintillation observations is that the spatial scales of irregularities can be investigated using the technique introduced by *Bhattacharyya et al.* [2003]. This technique has been used earlier to investigate the spatial scales of *F* region irregularities [*Engavale and Bhattacharyya*, 2005; *Bhattacharyya et al.*, 2014], but it is not applied to *E* region irregularities so far. This technique can be applied to both weak and strong scintillations to retrieve information about spatial scale of irregularities.

E_{sb} are frequently observed at midlatitudes as well, and their formation can be well explained with the wind-shear mechanism [*Whitehead*, 1961; *Axford*, 1963]. However, this mechanism fails at the dip equator due to the horizontal nature of the Earth's magnetic field close to the dip equator. The formation of E_{sb} near the dip equator is still an open question. Phenomena like E_s/E_{sb}, EEJ/CEEJ, Type I/II irregularities occur in a narrow altitudinal belt of *E* region, but the linkage between these processes is not yet well understood. In this context, the present study sheds some light on the structuring of *E* region irregularities and probable ambient conditions on EEJ/CEEJ days. The experimental setup and data analysis technique are described in section 2. Results are explained in section 3 and compared with theoretical model in section 4. The present work is discussed and concluded in section 5 and 6, respectively. The relation between decorrelation scale d_l [*Bhattacharyya et al.*, 2003] and Fresnel scale [*Briggs*, 1984] of irregularities is obtained theoretically and presented in the Appendix.

2. Experimental Setup and Data Analysis

In the present study, we have used spaced receiver scintillation observations on 251 MHz signal transmitted from geostationary satellite UFO2 located at 71.2°E. The zenith angle θ and azimuth angle A of the incoming signal are 12.8° and 216.9° respectively. Scintillations are recorded for every 0.1 s at dip equatorial station Tirunelveli (8.7°N, 77.8°E, dip latitude 0.6°N) by two receivers separated by a distance of $x_0 = 540$ m along the magnetic east-west direction. We examined the scintillation data from 2000–2006 to search for daytime scintillations, and we could get only seven daytime scintillation events. These scintillations were seen in the postnoon period of the day during June–July solstice of 2003–2005. All these seven days are geomagnetically quiet and have $\sum Kp \leq 19$. The phase perturbations (σ_ϕ^2) imposed on incoming radio signal are proportional to $\alpha(m)\lambda^2(\Delta N)^2$, where $\alpha(m)$ is a constant dependent on power spectral index m and λ is the wavelength of incoming radio signal. The occurrence of scintillation on 251 MHz during daytime is expected to be lower as ΔN is smaller due to low background electron density in the *E* region, which enforces smaller phase perturbations on the incoming VHF signal. It clearly indicates the sparseness of these observations.

The scintillation observations are subjected to the full cross-correlation analysis technique introduced by *Briggs* [1984], and the parameters S_4, V_0, V_C, $C_l(x_0, t_m)$ are estimated for every 3 min. S_4 is a measure of strength of scintillation, and it is defined as the standard deviation of normalized intensity variations. V_0 gives the drift of the ground scintillation pattern in the receivers' plane. Considering the geometry of incoming signal, we get $V_0 = V_x - V_z \tan\theta \sin A$, where V_x and V_z are the eastward and vertical drifts of irregularities, respectively. Substitution of θ and A in the expression for V_0 gives an amount of $-0.14V_z$ that contributes to V_0. When V_z is smaller, V_0 represents the zonal irregularity drift V_x, i.e., $V_0 \approx V_x$. Random velocity, V_C, is the measure of the changes in the irregularity characteristics. $C_l(x_0, t_m)$ is the maximum cross correlation between intensity variations between the two receivers. It should be noted that the estimates of V_0 and V_C are available only when $C_l(x_0, t_m) \geq 0.5$. This condition confirms that the form of space-time correlation function assumed in the analysis technique is valid. This technique has been used to get information on *F* region irregularities from spaced receiver scintillation observations [*Bhattacharyya et al.*, 1989, 2001; *Kakad et al.*, 2007, 2012]. In addition, we utilized ionograms recorded at every 15 min by ionosonde at Trivandrum (8.5°N, 76.6°E, dip latitude 0.5°N) to ascertain the presence of E_{sb}. The ionograms are manually examined to find the occurrence of E_{sb} and blanketing frequency (fbE_s), the minimum frequency at which the *F* region trace starts appearing in the ionograms. E_s with $fbE_s \geq 4.5$ MHz are considered as E_{sb}. Also, we used ground-based hourly observations of geomagnetic field's *H* component recorded at Tirunelveli and Alibag (18.6°N, 72.9°E, dip latitude 14.1°N) to get the temporal variation of EEJ. Alibag is an off-equatorial station and lies outside the influence of EEJ. Diurnal variation of the *H* component (ΔH) at each station is obtained by subtracting the local midnight hourly value from the respective 24 hourly values. EEJ is then calculated by subtracting hourly ΔH values of Alibag from corresponding hourly ΔH values of Tirunelveli [*Patil et al.*, 1990a, 1990b].

E region irregularities vary from few meters to hundreds of meters [*Gupta*, 1997a, 1997b, and references therein] and follow a power law spectrum, i.e., $\Phi(\Delta N) \propto k^{-p}$, where p is three-dimensional power spectral index. Estimation of spatial scale length of irregularities is crucial as fast-moving small-scale sized irregularities enhance the fading rate and cause more degradation of the incoming radio signal. In case of weak scintillations, power spectral analysis can be used to get the Fresnel frequency, which later can be converted to spatial scales with the knowledge of drift speed of the irregularity, i.e., $d_F = V_0/\nu_F$ [*Wernik et al.*, 1983; *Kakad et al.*, 2012]. Further, we computed the coherence scale present in the ground scintillation pattern using a new technique developed by *Bhattacharyya et al.* [2003], which is applicable to both weak and strong scintillations. The coherence scale d_l gives an estimate of the dominant spatial scale present in the ground scintillation pattern. The details of computation of d_l are given in *Engavale and Bhattacharyya* [2005]. The relation between Fresnel scale d_F and coherence scale d_l is derived theoretically and given in the Appendix.

We carried out power spectral analysis for the daytime scintillation events considered here and estimated the (i) Fresnel frequency ν_F and (ii) power spectral slopes $m = p-1$ for every 3 min. According to weak scintillation theory, the irregularities having a size of the order of Fresnel scale $\sqrt{2\lambda Z}$ contribute the maximum to weak scintillations [*Briggs*, 1975; *Yeh and Liu*, 1982], where Z is the height of irregularity layer and λ is the wavelength of incoming radio signal. Hence, in the power spectrum, the maximum power is associated with frequency $V_0/\sqrt{2\lambda Z}$. When irregularity layer is sufficiently thin, Fresnel oscillations are clearly visible in the power spectrum and we can estimate the frequencies associated with the first, second, etc., maxima/minima. Thus, with the knowledge of nth Fresnel frequency ν_{Fn} associated with the nth maximum/minimum and irregularity drift V_0, we can estimate the height of the irregularity layer using equations (1) and (2), respectively.

For the nth maximum,

$$Z = \frac{(2n-1)V_0^2}{2\lambda \nu_{Fn}^2} \tag{1}$$

For the nth minimum,

$$Z = \frac{nV_0^2}{\lambda \nu_{Fn}^2} \tag{2}$$

Here, $n = 1, 2, 3 \ldots$ represents the position of the maximum/minimum. In the present study, we have estimated the irregularity height using the frequency linked with the first Fresnel minimum (i.e., $n = 1$).

3. Results

We have divided daytime scintillation events into two categories depending on the presence/absence of CEEJ on that day. We find that four days, namely, 6 July 2003, 13 June 2004, 5 July 2005, and 8 July 2005 show presence of CEEJ. These are considered under Cat-I. The other three days, namely, 8 July 2003, 5 June 2004, and 14 June 2004 are considered under Cat-II, on which CEEJ was not seen.

3.1. Occurrence of Daytime VHF Scintillations

The temporal variation of S_4 index and EEJ for days falling under Cat-I and Cat-II is shown in Figure 1. Scintillations are considered to be above noise level when $S_4 \geq 0.15$, which is shown in Figures 1a and 1b by horizontal lines [*Kakad et al.*, 2012]. When $\mathrm{EEJ}_{\min} \leq -10$ nT, then it is chosen as a day with CEEJ. This limit is shown by horizontal lines in Figures 1c and 1d. It is seen that scintillations are present in a narrow window of time close to 12:00–18:00 India Standard Time (IST). Secondly, only June–July solstice of 2003–2005 is exhibiting daytime scintillations. Strong electron density irregularities are required to produce scintillations on 251 MHz, which are absent in the *F* region during daytime. Thus, *E* region irregularities in the presence of E_{sb} are the likely source for these daytime scintillations. To confirm the presence of E_{sb} on these days, we examined the ionosonde data recorded at a nearby station Trivandrum. On two days, namely, 6 July 2003 and 8 July 2003, ionosonde data were not available. For the remaining five days, the temporal variation of fbE_s is shown in Figure 2. The open (closed) symbols represent Cat-I (Cat-II) days. It is evident that the daytime scintillations are associated with presence of E_{sb}, and average blanketing frequency is found to be 7.49 ± 3.03 MHz. The higher (> 8 MHz) values of fbE_s depicted in Figure 2 correspond to total blanketing events.

E_s/E_{sb} are frequently observed at midlatitudes, and their inhomogeneities cause scintillations on VHF signal during daytime, mainly during summer season. Also, higher E_s critical frequency ($foE_s \geq 4$ MHz) is required for daytime scintillations [*Aarons and Whitney*, 1968; *Dasgupta and Kersley*, 1976]. E_s/E_{sb} is also observed at

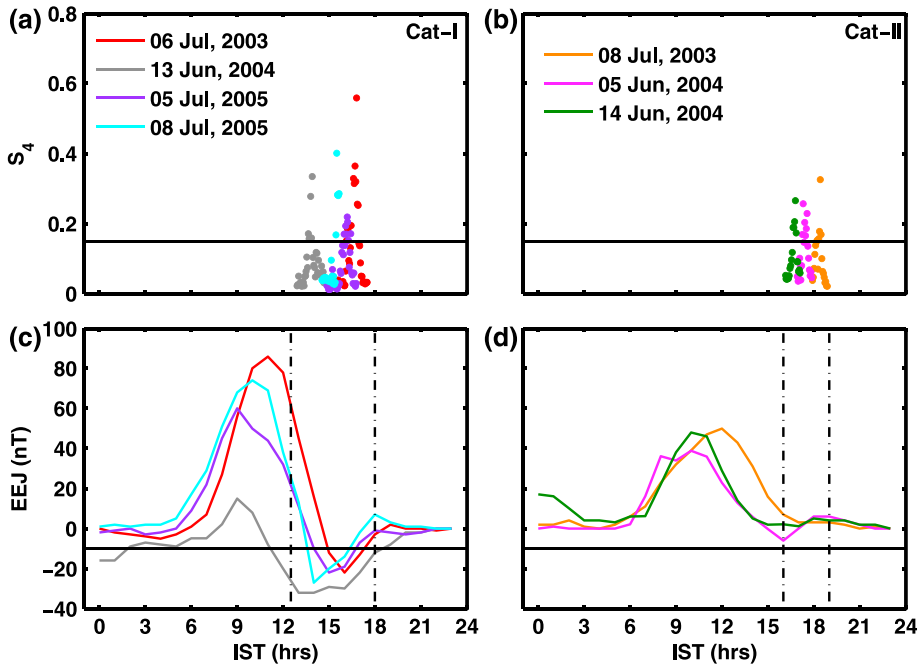

Figure 1. S_4 index for daytime VHF scintillation events on (a) Cat-I and (b) Cat-II days along with respective (c and d) EEJ profiles. The horizontal lines in Figures 1a and 1b represent $S_4 = 0.15$. The horizontal lines in Figures 1c and 1d represent EEJ = −10 nT.

equatorial/low-latitude stations, and their important feature is its peak occurrence during the local summer [*Chandra and Rastogi*, 1975; *Devasia*, 1976; *Devasia et al.*, 2006]. Recently, *Yadav et al.* [2014] used ionosonde observations from dip equatorial station Tirunelveli in Indian longitude and have shown that E_{sb} is more likely to occur during 13:00–18:00 IST with a peak occurrence at around 16:00 IST during the summer solstice. The occurrence of daytime scintillations during postnoon period and their close association with E_{sb} is in general agreement with earlier studies [*Basu et al.*, 1977; *Rastogi and Mullen*, 1981].

3.2. *E* Region Irregularity Drift Speed

Temporal variations of the other parameters obtained from scintillation data, viz., $C_l(x_0, t_m)$, V_C, and V_0 are shown in Figure 3 for Cat-I (open symbols) and Cat-II (closed symbols). The maximum cross correlation between intensity variations recorded by two receivers, $C_l(x_0, t_m)$, is well above 0.7 for most of the events. It

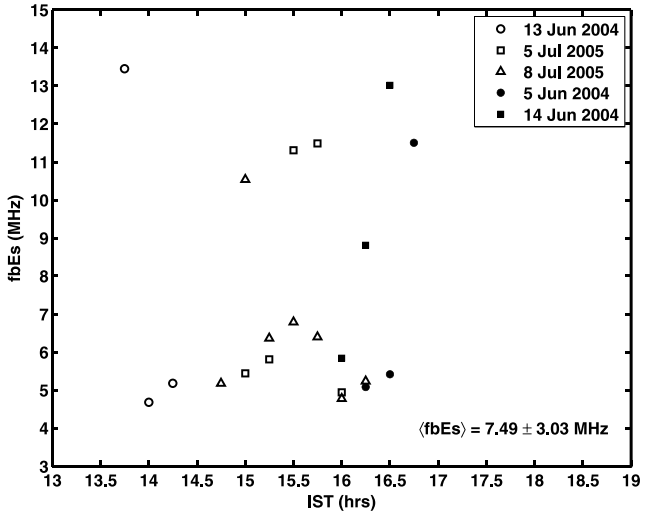

Figure 2. fbE_s on Cat-I (open symbols) and Cat-II (closed symbols) days. $fbE_s > 8$ MHz are total blanketing events.

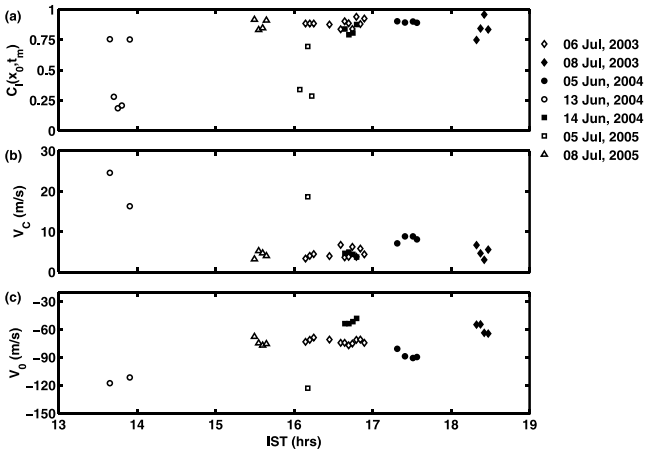

Figure 3. (a) Cross-correlation function $C_I(x_0, t_m)$, (b) random velocity V_c, and (c) drift velocity V_0 as a function of IST are shown for Cat-I (open symbols) and Cat-II (closed symbols) days.

indicates that the characteristics of the irregularities producing these scintillations are not changing rapidly, and hence, these irregularities are not in the early phase of their development [*Bhattacharyya et al.*, 2001]. Random velocity, V_C, is a measure of random changes in irregularity characteristics and is shown in Figure 3b. Lower values of V_C (<10 m/s) also confirm that the irregularity characteristics are not changing rapidly. Drift speed of ground scintillation pattern, V_0, is determined by the movement of irregularities across the signal path. For irregularities situated at 100 km, the estimate of Fresnel scale comes out to be 489 m. Thus, it should be noted that the drift speeds estimated from these scintillations are associated with *E* region irregularities having a size of few hundreds of meters. In the case of *E* region, electrons and ions possess differential motions, and hence, V_0 estimated from daytime VHF scintillations gives the *E* region irregularity drift. When the irregular medium is changing significantly, the estimated V_0 can over or under estimate the irregularity drift as $V_0 = V_x + 0.14V_z$. However, when V_C is small, V_0 represents the average phase speed, $V_{ph'}$ of long wavelength structures generated through gradient drift instability in the *E* region, which is given by *Fejer et al.* [1975].

The temporal variation of V_0 is shown in Figure 3c. It is found that the irregularities producing the scintillations are drifting westward with a speed of 40–70 m/s. A strong westward irregularity drift of ≈ 120 m/s is observed on the strongest CEEJ (≈ −32 nT) day, 13 June 2004. It should be noted that $V_{ph'}$ is the speed of irregularities in the neutral frame of reference, whereas V_0 (≈ −120 to −40 m/s) represents the phase speed of irregularities in the receivers' frame of reference. Typical parameters for *E* region yield $V_{ph'}$ in the range of −50 to −30 m/s for long wavelengths (>100 m). This suggests that neutrals are moving with a speed of −90 to 10 m/s. It indicates that neutral wind was westward during these events.

Earlier studies using MF, VHF, Meteor and Coherent scatter radars have demonstrated that winds/irregularity drifts are highly variable in the dynamic region of 80–120 km [*Somayajulu et al.*, 1993, 1994a; *Gurubaran and Rajaram*, 1999; *Ramkumar et al.*, 2010]. The westward irregularity drifts observed here are in agreement with *Somayajulu et al.* [1994b]. *Patra et al.* [2014] have used observations from newly installed 30 MHz radar at Gadanki (13.5°N, 79.2°E; 6.5°N magnetic latitude) and shown that daytime zonal velocities of 10 m sized *E* region irregularities are eastward (westward) with values as high as 80 m/s (20 m/s) in the lower (upper) echoing region. How do *E* region irregularity drifts compare to zonal winds at that altitude has not been examined yet. *Somayajulu et al.* [1993] have shown that the winds vary considerably with altitude and are westward above 100 km during the postnoon period. *Shume et al.* [2005] have used Type II radar echoes observed at Jicamarca Radio Observatory in Peru and shown that the neutral winds are westward (<100 m/s) above 105 km in the postnoon period. It suggests that the irregularity zonal drift and neutral winds are both westward above 100 km.

3.3. Power Spectral Characteristics of *E* Region Irregularities

Power spectrum analysis of the scintillation data is carried out to obtain (i) power spectral slopes (*m*), (ii) Fresnel frequencies associated with the first and second minima, and (iii) presence/absence of Fresnel oscillations for every 3 min. Examples of power spectrum are shown in Figures 4a–4d (Figures 4e–4h) for Cat-I (Cat-II) days. The vertical arrows marked in each subfigure indicate the first and second Fresnel minima.

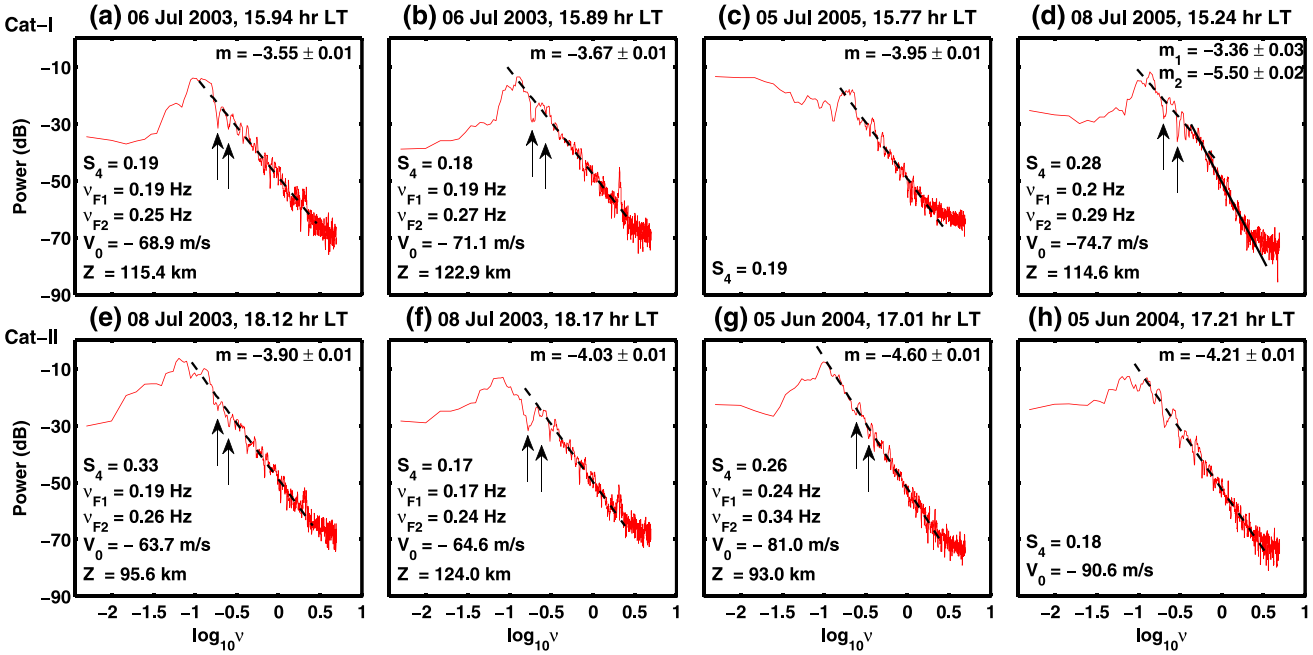

Figure 4. Power spectra on (a–d) Cat-I and (e–h) Cat-II days. The broken lines represent the slope (m) of the power spectra. The arrows represent the first and second frequency minima of Fresnel oscillations. Scintillation strength S_4, drift velocity V_0, first and second Fresnel frequencies ν_{F1} and ν_{F2}, and power spectral slope m are mentioned in each subplot. The height of the irregularity layer, Z, calculated from first Fresnel minimum is also mentioned. Note the break-in slope (slopes given by m_1 and m_2) in Figure 4d.

The corresponding values of S_4, V_0, m, and Z_{cal} are also mentioned in each plot. The cases for which Fresnel oscillations are not seen, ν_F, is not mentioned. Sometimes break-in power spectrum is observed for days falling under Cat-I. One such example is shown in Figure 4d. Such break-in-power spectra are not observed for Cat-II days. It is observed that irregularity spectrum has maximum power close to Fresnel frequency, which falls of linearly as frequency increases. The irregularity spectra shown in Figure 4 are in agreement with earlier observed E region spectra [*Bhattacharyya*, 1991] with frequency contributions from 0.1–1 Hz. The corresponding power ranges from −10 to −50 dB. It is noticed that the days of Cat-I are mostly associated with lower values of power spectral slope as compared to those of Cat-II. It suggests that E region irregularities possess shallower power spectrum and hence support the presence of comparatively smaller-scale irregularities on CEEJ days.

Equation (2) indicates that the Fresnel frequency associated with the nth minimum is proportional to $\sqrt{n}$. Thus, the theoretical ratio of the first to second Fresnel minima $r_{theory} = \nu_{F1}/\nu_{F2}$ comes out to be 0.7071. To confirm the presence of Fresnel oscillations, we computed the ratio of the first to second Fresnel frequencies, i.e., r_{obs} from the power spectrum and compared it with r_{theory}. In Figure 5a, r_{obs} is shown for each 3 min scintillation event. A power spectrum is considered to have Fresnel oscillations only if r_{obs} lies within ±6% deviation from $r_{theory} = 0.7071$. It is found that 56% of scintillation events show Fresnel oscillations, which indicates presence of thin layer of irregularity at E region altitude [*Yeh and Liu*, 1982]. Further, we converted the Fresnel frequency into spatial scales and computed the height, Z_{cal} of irregularity layer using equation (2). However, it should be noted that Z_{cal} represents the slant height of the irregularity layer, as the zenith angle of the incoming VHF signal is 12.8°. The estimated slant height of irregularity layer is shown as a function of IST in Figure 5b. The average slant height is found to be $\langle Z_{cal} \rangle = 117 \pm 13$ km. The average vertical height is given by $Z = Z_{cal} \cos\theta$ and comes out to be 114 ± 13 km. It confirms that the source irregularities that caused the observed scintillations are indeed situated in the E region. Since an amount of $-0.14V_Z$ contributes to V_0, occasionally, the estimated V_0 can give rise to comparatively higher value of Z_{cal} that is seen as outlier in Figure 5b. Since this point with $Z_{cal} \approx 200$ km is statistically an outlier, it is not considered for computing the average height of irregularity layer.

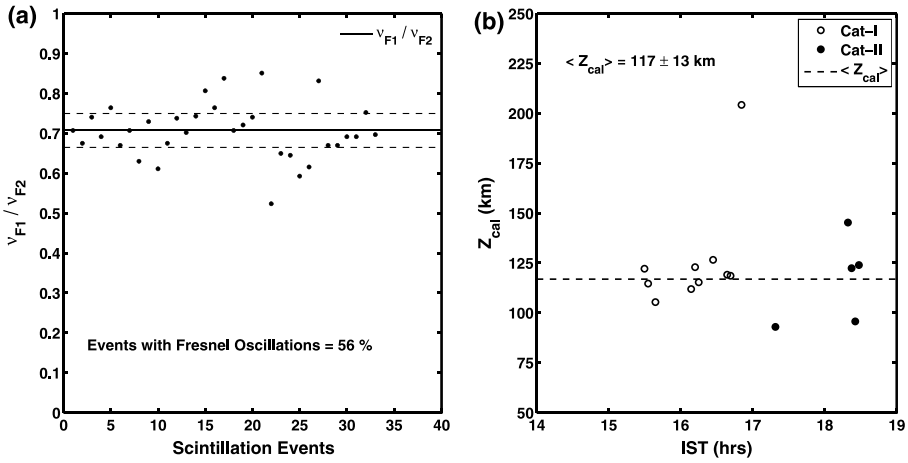

Figure 5. (a) Statistics of scintillation events exhibiting Fresnel oscillation in power spectra. The black circles are observed values of ν_{F1}/ν_{F2}. The solid horizontal line gives the theoretical estimates for ratio ν_{F1}/ν_{F2}, and the dashed lines represent 6% deviation from this theoretical value. (b) Z_{cal}, slant height of the irregularity obtained from first Fresnel minimum as a function of IST. Vertical height of the irregularity, $Z_{\perp} = Z_{cal} \cos\theta = 114 \pm 13$ km.

3.4. Spatial Scales of *E* Region Irregularities

Bhattacharyya et al. [2003] have developed a new technique to retrieve information about spatial scales of irregularities, which is applicable for both weak and strong scintillations. We applied this technique and estimated the coherence scale (d_l) present in the ground scintillation pattern. The coherence scale is the measure of the dominant spatial scale length present in the ground scintillation pattern and is given by equation (3).

$$C_l(X = d_l, t = 0) = 0.5 \tag{3}$$

It should be noted that the form of spatial correlation function $C_l(X)$, which is unknown, is essential to compute the coherence scale. In this technique the $C_l(X)$ is obtained by plotting $C_l(x_0, t_m)$ as a function of $x_0 V_C/(V_0{}^2 + V_C{}^2)^{1/2}$, which is shown for Cat-I and II days in Figures 6a and 6b, respectively. It is assumed that the spatial correlation function follows a Gaussian given by equation (4), where l_0 is the outer scale. The continuous and dotted lines depicted in Figures 6a and 6b correspond to the average and smallest/largest coherence scale obtained from the Gaussian fit.

$$C_l(X) = e^{\left(\frac{-X^2}{l_0^2}\right)} \tag{4}$$

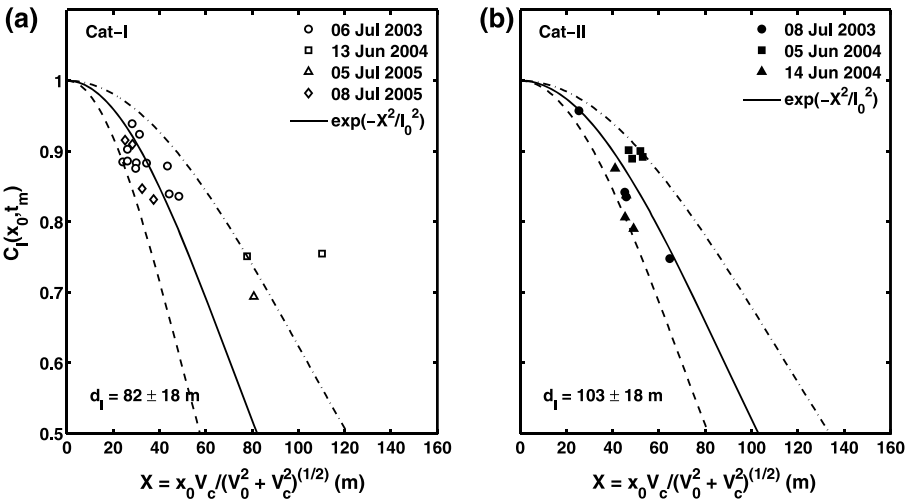

Figure 6. Determination of d_l from $C_l(x_0, t_m)$ versus $x_0 V_C/(V_0{}^2 + V_C{}^2)^{1/2}$ plot of all scintillation events on (a) Cat-I and (b) Cat-II days. The dotted and continuous lines represent the smallest/largest and average coherence scale obtained from Gaussian fit.

Table 1. Input Parameters Used in the Theoretical Model of *Engavale and Bhattacharyya* [2005]

Parameter	Value	Details
Height of irregularity (Z)	110 km	Ionosonde Observations
Plasma Frequency (f_p)	7.5 MHz	Ionosonde Observations
Thickness of irregularity (T)	5 km	
Number of phase screens (n_z)	1	
Single power spectral index (m)	2, 3, 4, 5	
Break-in power spectral indices (m_1, m_2)	2, 4 and 2, 6	
Outer scale (R_0)	1000 m	Applicable for all m
Inner scale (r_0)	10 m	Applicable for $m = 2$
Break-in scale (R_b)	200 m	Applicable for break-in power spectra
Density fluctuation (ΔN)	6–19%	

The average coherence scale for Cat-I and Cat-II is found to be 82 ± 18 m and 103 ± 18 m, respectively. It is evident that the average coherence scale varies considerably for CEEJ and non-CEEJ days. It particularly points toward the differences in *E* region background conditions on CEEJ and non-CEEJ days, which might be playing an important role in controlling the coherence scales.

4. Validation of Coherence Scale With Theoretical Model

Development of scintillations during propagation of radio waves through irregular medium is governed by various physical characteristics of the irregularities like thickness, height, ambient plasma density, density fluctuations, and power spectrum. To examine the various ionospheric conditions responsible for the observed daytime VHF scintillation, we used the theoretical model developed by *Engavale and Bhattacharyya* [2005]. The model assumes that a plane wave of unit amplitude is incident on an irregularity layer of thickness T located at an altitude Z. It uses the "split step" method given by *Bhattacharyya and Yeh* [1988] in which the medium containing the irregularities is divided into a number of thin phase screens separated by free space. By considering different power spectral indices for *E* region irregularities, the variation of S_4 index and spatial correlation function $C_l(x)$ in the receivers' plane is explored using this theoretical model. The input parameters used in the theoretical model are given in Table 1. We assumed the irregularities to be at a height of 110 km with ambient plasma density of 7.5 MHz. Various power spectral indices are chosen in the range of 2–6 including break-in slopes. The density perturbation ΔN is varied from 6–19% such that S_4 is maintained within weak scintillation regime, $0.15 \leq S_4 \leq 0.4$, and profiles of $C_l(x)$ are obtained.

The output $C_l(x)$ as a function of x is shown in Figure 7 for spectral indices m = (a) 2, (b) 3, (c) 4, (d) 5, and break-in slope (e) $m_1 = 2, m_2 = 4$ and (f) $m_1 = 2, m_2 = 6$. The range of phase perturbations, σ_ϕ, associated with these profiles is mentioned in each plot. It should be noted that for weak scintillations σ_ϕ lies in the range of 0.16 to 0.78 radians, which is in agreement with earlier theoretical studies [*Booker and Majidiahi*, 1981]. It is found that $C_l(x)$ follows nearly the same pattern and tends to produce the same coherence scale on ground for weak scintillations. However, these coherence scales are found to be dependent on the irregularity power spectral index m. We have estimated the average coherence scale using the theoretical model for the above mentioned spectral indices and compared them with observed d_l. Figure 8 shows the coherence scale as a function of power spectral index m obtained from the theoretical model and observations. It should be noted that the coherence scale obtained from the scintillation represents the projection of irregularity scale length perpendicular to the signal path in the receivers' plane. Hence, the coherence scale obtained from scintillation observations is divided by cos θ while comparing with the theoretical results. It is marked that the coherence scale increases with the power spectral index m for a fixed height. The model suggests a presence of 6–19% density perturbations in the *E* region. The average fbE_s comes out to be 5.5 ± 0.64 MHz, when we exclude total blanketing events ($fbE_s \geq 8$ MHz). For this case, the theoretical model suggests a presence of 10–35% density perturbations, which is higher as compared to earlier reports of 5–15% density perturbations

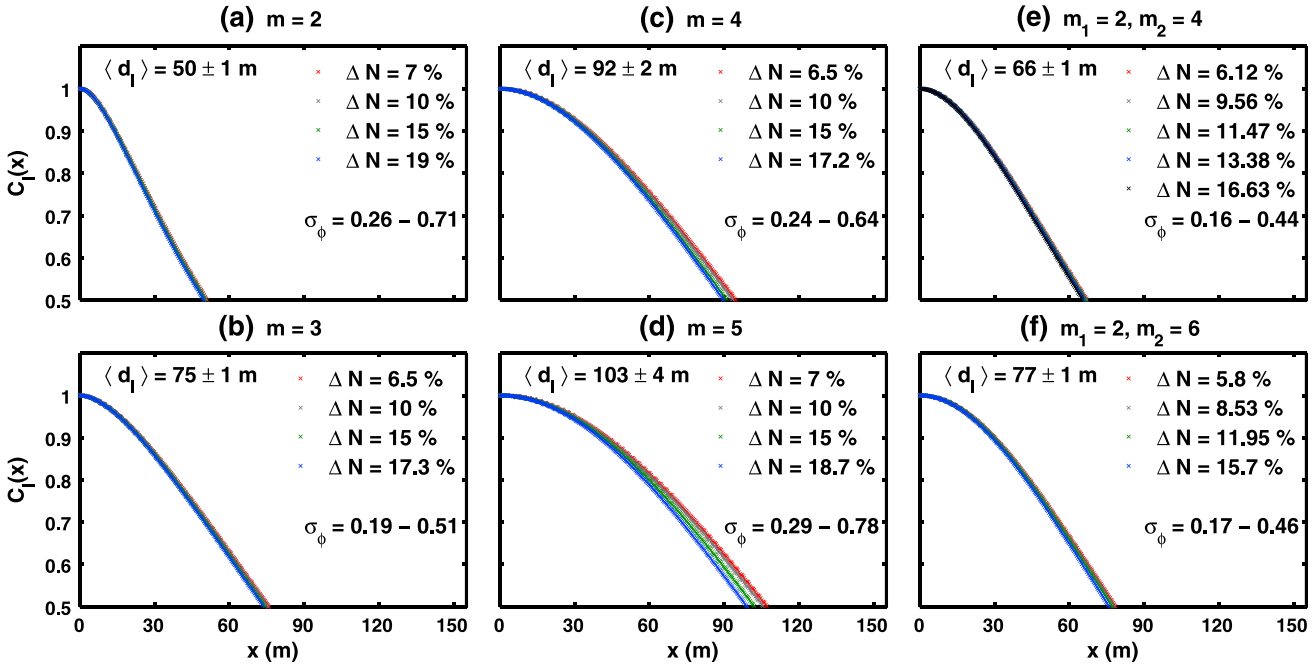

Figure 7. Spatial correlation function $C_l(x)$ obtained by changing density perturbation (ΔN), using model given by *Engavale and Bhattacharyya* [2005] for weak scintillations ($0.15 \leq S_4 \leq 0.4$) and their profiles for various power spectral slopes (m). (e) and (f) show the profiles for break-in power spectra. σ_ϕ mentioned in each subplot is in radian.

in the EEJ region [*Basu et al.*, 1977; *Pfaff et al.*, 1987]. Thus, theory and observations, both, confirm presence of smaller-scale-sized irregularities in the *E* region on CEEJ days as compared to that on non-CEEJ days.

The relation between coherence scale and Fresnel scale has been derived in the Appendix. It is found that $d_l = d_F/6$. Using this relation, we get $d_F = 492$ m and 618 m for CEEJ and non-CEEJ days, respectively. It is in close accordance with theoretical estimates of Fresnel scale for $Z = 100$ km.

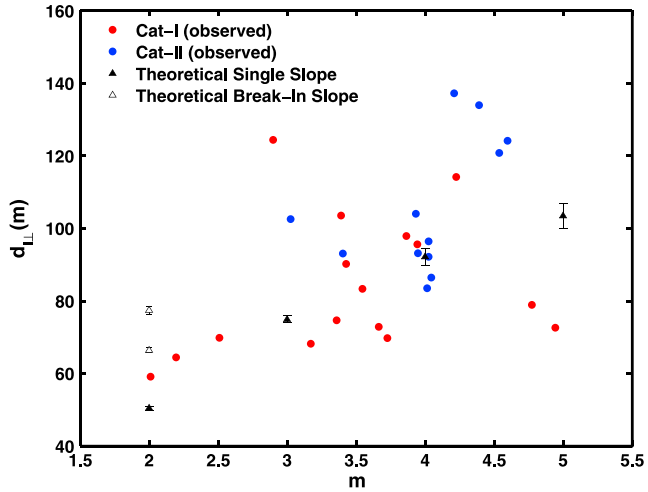

Figure 8. Comparison of coherence scale d_l as a function of irregularity power spectral index (m) obtained from the model given by *Engavale and Bhattacharyya* [2005] and the daytime scintillation observations. $d_{l\perp} = d_l/\cos\theta$ obtained from observations on Cat-I and Cat-II days are represented by red and blue circles, respectively. Closed and open triangles represent d_l obtained from model runs with single and two-component power spectral index and hence single and break-in slopes, respectively.

5. Discussion

The key to why the structuring of *E* region irregularities is considerably different on CEEJ and non-CEEJ days probably lies in the background conditions present on those days. Two-stream and gradient drift instabilities are the main source for the formation of irregularities in the *E* region [*Farley*, 1963; *Buneman*, 1963; *Schmidt and Peter Gary*, 1973, and references therein]. In earlier studies it is shown that the irregularities formed through gradient drift instability have longer wavelength [*Schmidt and Peter Gary*, 1973, and references therein]. As mentioned earlier, the observed VHF scintillations are linked with the *E* region irregularities of the order of few hundred meters. Thus, it is clear that they are associated with gradient drift instability. For the equatorial electrojet plasma waves, the linear growth rate of the waves caused by two-stream and gradient drift instabilities is [*Farley and Fejer*, 1975; *Farley*, 2009]:

$$\gamma = -2\alpha n_0 + \frac{1}{(1+\psi)}\left\{\frac{\psi}{\nu_i}\text{term1} + \frac{1}{Lk^2}(\text{term2} + \text{term3})\right\} \tag{5}$$

where

$$\begin{aligned}\text{term1} &= (\omega_r - kV_{Di})^2 - k^2{C_s}^2 \\ &= \left(\frac{kV_{De} + k\psi V_{Di} - kV_{Di} - k\psi V_{Di}}{1+\psi}\right)^2 - k^2{C_s}^2 \\ &= \frac{k^2}{1+\psi^2}(V_{De} - V_{Di})^2 - k^2{C_s}^2 \\ &= \frac{k_y}{1+\psi_0}(V_{De} - V_{Di}) - k^2{C_s}^2\end{aligned}$$

$$\begin{aligned}\text{term2} &= (\omega_r - kV_{Di})\left(\frac{\nu_i}{\Omega_i}k_y + \psi_0 k_z\right) \\ &= \frac{k_y}{1+\psi}(V_{De} - V_{Di})\left(\frac{\nu_i}{\Omega_i}k_y\right) \\ &= \frac{\nu_i k^2}{(1+\psi)\Omega_i}(V_{De} - V_{Di})\end{aligned}$$

$$\begin{aligned}\text{term3} &= -(\omega_r - kV_{De})\left(\frac{\nu_i\Omega_i}{{\nu_i}^2 + {\omega_l}^2}k_y - k_z\right) \\ &= -(\omega_r - kV_{De})\left(\frac{\nu_i\Omega_i}{{\nu_i}^2 + {\omega_l}^2}\right)k_y\end{aligned}$$

The vertical electron density gradient length is positive for densities increasing with altitude (usual daytime condition).

$$L = n_0\left(\frac{\partial n}{\partial Z}\right)^{-1} \tag{6}$$

The ion acoustic velocity is

$$C_s = \left[\frac{K_B(\nu_e T_e + \nu_i T_i)}{m_i}\right]^{\frac{1}{2}} \tag{7}$$

Equation (5) has two driving terms and two limiting cases, giving rise to two different instabilities [*Farley*, 2009]. Recombination is unimportant for wavelengths of a few meters or less. The relative drift speed of electrons with respect to ions is ΔV_d and is given by $V_{De} - V_{Di}$. When ΔV_d exceeds C_s, term1 is much greater than term2 + term3 and we get two-stream instability. This instability produces Type I radar echoes. When ΔV_d is much less than C_s but not zero, term2 + term3 will be larger than term1, resulting in gradient drift instability. Generally, Type II radar echoes are produced by gradient drift instability.

Solution of equation (5) indicates that three parameters, namely, (i) lower $L = n_0\left(\frac{\partial n}{\partial Z}\right)^{-1}$, (ii) lower ΔV_d, and (iii) higher electron temperature can cause the growth rate to be positive at longer wavelengths. Thus, we propose that on CEEJ days, *L* might be higher or ΔV_d might be higher or electron temperature might be lower to produce relatively small-scale structures as compared to that on non-CEEJ days. Recently, *Vineeth et al.* [2012] have reported a decrease in neutral temperature during CEEJ, which is consistent with our results.

6. Conclusions

Here we have studied sparse daytime scintillation observed on 251 MHz recorded by spaced receivers at dip equatorial station Tirunelveli in Indian longitude. The scintillations are found to occur during postnoon period of June–July solstice of moderate to low solar activity period and are closely linked with E_{sb}, which is in general agreement with the earlier studies [*Basu et al.*, 1977; *Rastogi and Mullen*, 1981; *Bhattacharyya and Rastogi*, 1986; *Bhattacharyya*, 1991]. For the first time, the spatial scales of *E* region irregularities are examined using the technique introduced by *Bhattacharyya et al.* [2003]. The main conclusions of the study are as follows:

1. Earlier works on daytime scintillations were carried out using single receiver scintillation observations. However, this is the first study using spaced receiver scintillation observations. Its advantage is that one can examine the spatial scales of *E* region irregularities.
2. These irregularities (Type I/Type II) have been mostly studied using radar observations that are associated with small-scale (3 m, 8.33 m, etc.) irregularity structures. Using VHF scintillations, we have examined the spatial scale lengths of longer wavelength (100 m to 1 km) *E* region irregularity structures during CEEJ and non-CEEJ days, which are not well explored. The present study also demonstrates that daytime spaced receiver scintillation observations have potential to contribute to the understanding of long wavelength *E* region irregularities.
3. Through power spectral analysis, it is confirmed that the daytime scintillations are caused due to irregularities situated in the *E* region at an altitude of 114 ± 13 km.
4. It is found that the irregularities producing scintillations are drifting westward with speeds of 40–70 m/s. Irregularity drifts are substantially westward on a day having stronger CEEJ. The present study demonstrates that daytime spaced receiver observations can be used as a tool to get the zonal drift of *E* region irregularities.
5. The spatial scale lengths linked with *E* region irregularities are found to be smaller on CEEJ days as compared to those on non-CEEJ days.
6. Coherence scale lengths obtained from scintillation observations are validated with the theoretical model proposed by *Engavale and Bhattacharyya* [2005]. The relation between Fresnel scale and coherence scale is derived, and it is found that $d_F = 6d_l$.
7. Theoretical model suggests that 6–19% density perturbations are required to produce weak scintillations ($S_4 \leq 0.4$) on 251 MHz, which are in accordance with earlier observations in EEJ region [*Basu et al.*, 1977; *Pfaff et al.*, 1987].

The present exercise reveals that daytime irregularity drifts derived from spaced receiver scintillation observation can serve as proxy for *E* region irregularity drifts. More such observations can help to explore the dynamics and evolution of longer wavelength *E* region irregularities, which are not yet understood well.

Appendix A: Relation Between Coherence Scale (d_l) and Fresnel Scale (d_F)

According to *Briggs* [1975], a plane wavefront, when passing through the ionosphere, encounters random changes in the refractive index due to presence of density irregularities. In this study, it is found that the phase variation across the emerging wavefront is sinusoidal, i.e.,

$$\phi(x) = \phi_1 \cos\left(\frac{2\pi x}{d_F}\right) \tag{A1}$$

where d_F, called Fresnel scale, gives the scale size of the irregularities that are most effective in producing amplitude scintillations on the ground. As the modulated phase front propagates away from the screen, amplitude perturbations are developed, which are given by

$$A(x) = 1 + A_1 \cos\left(\frac{2\pi x}{d_F}\right) \tag{A2}$$

The variation of the wavefield $E(x)$ across the wavefront is given as

$$E(x) = Ae^{i\phi(x)} \tag{A3}$$

then the intensity will be

$$I(x) = E(x)E^*(x)$$

$$I(x) = 1 + 2A_1 \cos\left(\frac{2\pi x}{d_F}\right) \tag{A4}$$

The correlation function for intensity is given by

$$B_I(x) = \langle I(x_1) I(x_1 + x) \rangle \tag{A5}$$

Using equations (A4) and (A5), we get

$$B_I(x) = 1 + 2A_1^2 \cos\left(\frac{2\pi x}{d_F}\right) \tag{A6}$$

In the theoretical model given by *Engavale and Bhattacharyya* [2005], the one-dimensional space-time correlation function is given by

$$C_I(x) = \frac{B_I(x) - 1}{B_I(0) - 1} \tag{A7}$$

Substituting equation (A6) in equation (A7),

$$C_I(x) = \cos\left(\frac{2\pi x}{d_F}\right) \tag{A8}$$

Coherence scale d_I is the spatial lag at which the spatial correlation falls to half of its maximum value of unity, i.e., when $C_I(x) = 0.5$, $x = d_I$. Substituting these values in equation (A8)

$$0.5 = \cos\left(\frac{2\pi d_I}{d_F}\right)$$

$$d_F = 6d_I \tag{A9}$$

Acknowledgments
We are thankful to K. Jeeva and K.U. Nair for their technical support on scintillation experiment. VHF scintillation and ionosonde data are available with the authors. EEJ is calculated using magnetic field component observations obtained from World Data Centre for Geomagnetism, Mumbai (http://wdciig.res.in/).

Alan Rodger thanks Aramesha Seif and two other reviewers for their assistance in evaluating this paper.

References

Aarons, J., and H. E. Whitney (1968), Ionospheric scintillations at 136 MHz from a synchronous satellite, *Planet. Space Sci.*, *16*, 21–28.
Anastassiadis, M., and D. Matsoukas (1970), 40-MHz ionospheric scintillation and the sporadic-*E* layer, *Radio Sci.*, *5*(6), 953–957.
Axford, W. I. (1963), The formation and vertical movement of dense ionized layers in the ionosphere due to neutral wind shears, *J. Geophys. Res.*, *68*, 769–779, doi:10.1029/JZ068i003p00769.
Basu, S., J. Aarons, and B. Balsley (1977), On the nature of the electrojet irregularities responsible for daytime VHF scintillations, *J. Geophys. Res.*, *82*, 5262–5266.
Bhattacharyya, A. (1991), Phase and amplitude scintillations due to electrojet irregularities, *J. Atmos. Terr. Phys.*, *53*(5), 379–387, doi:10.1016/0021-9169(91)90033-4.
Bhattacharyya, A., and R. G. Rastogi (1986), Multifrequency spectra of day-time ionospheric amplitude scintillations near the dip equator, *J. Atmos. Terr. Phys.*, *48*(5), 463–469, doi:10.1016/0021-9169(86)90123-6.
Bhattacharyya, A., and K. C. Yeh (1988), Intensity correlation function for waves of different frequencies propagating through a random medium, *Radio Sci.*, *23*(5), 791–808.
Bhattacharyya, A., S. J. Franke, and K. C. Yeh (1989), Characteristic velocity of equatorial F region irregularities determined from spaced receiver scintillation data, *J. Geophys. Res.*, *94*(A9), 11,959–11,969, doi:10.1029/JA094iA09p11959.
Bhattacharyya, A., S. Basu, K. M. Groves, C. E. Valladares, and R. Sheehan (2001), Dynamics of equatorial *F* region irregularities from spaced receiver scintillation observations, *Geophys. Res. Lett.*, *28*(1), 119–122, doi:10.1029/2000GL012288.
Bhattacharyya, A., K. M. Groves, S. Basu, H. Kuenzler, C. E. Valladares, and R. Sheehan (2003), L-band scintillation activity and space-time structure of low-latitude UHF scintillations, *Radio Sci.*, *38*(1), 1004, doi:10.1029/2002RS002711.
Bhattacharyya, A., B. Kakad, S. Sripathi, K. Jeeva, and K. U. Nair (2014), Development of intermediate scale structure near the peak of the *F* region within an equatorial plasma bubble, *J. Geophys. Res. Space Physics*, *119*, 3066–3076, doi:10.1002/2013JA019619.
Booker, H. G., and G. Majidiahi (1981), Theory of refractive scattering in scintillation phenomena, *J. Atmos. Terr. Phys.*, *43*(11), 1199–1214, doi:10.1016/0021-9169(81)90035-0.
Briggs, B. H. (1975), Ionospheric irregularities and radio scintillations, *Contemp. Phys.*, *16*(5), 469–488, doi:10.1080/00107517508210825.
Briggs, B. H. (1984), The analysis of spaced sensor records by correlation techniques, in *Middle Atmosphere Program, Handbook for MAP*, vol. 13, edited by R. A. Vincent, pp. 166–186, ICSU, Paris.
Buneman, O. (1963), Excitation of field aligned sound waves by electron streams, *Phys. Rev. Lett.*, *10*, 285–287, doi:10.1103/PhysRevLett.10.285.
Chandra, H., and R. G. Rastogi (1975), Blanketing sporadic *E* layer near the magnetic equator, *J. Geophys. Res.*, *80*, 149–153.
Dasgupta, A., and L. Kersley (1976), Summer daytime scintillation and sporadic *E*, *J. Atmos. Terr. Phys.*, *38*(6), 615–618, doi:10.1016/0021-9169(76)90157-4.
Devasia, C. V. (1976), Blanketing sporadic-*E* characteristics at the equatorial stations of Trivandrum and Kodaikanal, *Indian J. Radio Space Phys.*, *5*, 217–220.

Devasia, C. V., N. Jyoti, K. S. V. Subbarao, D. Tiwari, C. Raghava Reddi, and R. Sridharan (2004), On the role of vertical electron density gradients in the generation of type II irregularities associated with blanketing E_s(E_{sb}) during counter equatorial electrojet events: A case study, *Radio Sci.*, *39*, RS3007, doi:10.1029/2002RS002725.

Devasia, C. V., V. Sreeja, and S. Ravindran (2006), Solar cycle dependent characteristics of the equatorial blanketing E_s layers and associated irregularities, *Ann. Geophys.*, *24*, 2931–2947.

Ecklund, W. L., D. A. Carter, and B. B. Balsley (1981), Gradient drift irregularities in mid-latitude sporadic *E*, *J. Geophys. Res.*, *86*(A2), 858–862, doi:10.1029/JA086iA02p00858.

Engavale, B., and A. Bhattacharyya (2005), Spatial correlation funtion of intensity variations in the ground scintillation pattern produced by equatorial spread-*F* irregularities, *Indian J. Radio Space Phys.*, *34*, 23–32.

Farley, D. T., Jr. (1963), A plasma instability resulting in field-aligned irregularities in the ionosphere, *J. Geophys. Res.*, *68*, 6083–6097, doi:10.1029/JZ068i022p06083.

Farley, D. T. (2009), The equatorial *E*-region and its plasma instabilities: A tutorial, *Ann. Geophys.*, *27*(4), 1509–1520, doi:10.5194/angeo-27-1509-2009.

Farley, D. T., and B. B. Balsley (1973), Instabilities in the equatorial electrojet, *J. Geophys. Res.*, *78*(1), 227–239, doi:10.1029/JA078i001p00227.

Farley, D. T., and B. G. Fejer (1975), The effect of the gradient drift term on type 1 electrojet irregularities, *J. Geophys. Res.*, *80*(22), 3087–3090, doi:10.1029/JA080i022p03087.

Fejer, B. G., D. T. Farley, B. B. Balsley, and R. F. Woodman (1975), Vertical structure of the VHF backscattering region in the equatorial electrojet and the gradient drift instability, *J. Geophys. Res.*, *80*(10), 1313–1324, doi:10.1029/JA080i010p01313.

Gupta, S. P. (1997a), Thin layers of ionization observed by rocketborne probes in equatorial *E* region, *Adv. Space Res.*, *19*(1), 169–173, doi:10.1016/S0273-1177(96)00048-8.

Gupta, S. P. (1997b), Features of *E* region irregularities at the magnetic equator and in its vicinity, *Adv. Space Res.*, *20*(11), 2195–2198, doi:10.1016/S0273-1177(97)00670-4.

Gurubaran, S., and R. Rajaram (1999), Long-term variability in the mesospheric tidal winds observed by MF radar over Tirunelveli (8.7°N, 77.8°E), *Geophys. Res. Lett.*, *26*(8), 1113–1116, doi:10.1029/1999GL900171.

Hanuise, C. (1983), High-latitude ionospheric irregularities: A review of recent radar results, *Radio Sci.*, *18*(6), 1093–1121, doi:10.1029/RS018i006p01093.

Kakad, B., K. Jeeva, K. U. Nair, and A. Bhattacharyya (2007), Magnetic activity linked generation of nighttime equatorial spread *F* irregularities, *J. Geophys. Res.*, *112*, A07311, doi:10.1029/2006JA012021.

Kakad, B., C. K. Nayak, and A. Bhattacharyya (2012), Power spectral characteristics of ESF irregularities during magnetically quiet and disturbed days, *J. Atmos. Sol. Terr. Phys.*, *81-82*, 41–49, doi:10.1016/j.jastp.2012.04.008.

Ledvina, B. M., P. M. Kintner, and E. R. de Paula (2004), Understanding spaced-receiver zonal velocity estimation, *J. Geophys. Res.*, *109*, A10306, doi:10.1029/2004JA010489.

Patil, A. R., D. R. K. Rao, and R. G. Rastogi (1990a), Equatorial electrojet strengths in the Indian and American sectors. Part I. During low solar activity, *J. Geomagn. Geoelec.*, *42*, 801–811.

Patil, A. R., D. R. K. Rao, and R. G. Rastogi (1990b), Equatorial electrojet strengths in the Indian and American sectors. Part II. During high solar activity, *J. Geomagn. Geoelec.*, *42*, 813–823.

Patra, A. K., P. Srinivasulu, P. P. Chaitanya, M. D. Rao, and A. Jayaraman (2014), First results on low-latitude *E* and *F* region irregularities obtained using the Gadanki Ionospheric Radar Interferometer, *J. Geophys. Res. Space Physics*, *119*, 10,276–10,293, doi:10.1002/2014JA020604.

Pfaff, R. F., M. C. Kelley, E. Kudeki, B. G. Fejer, and K. D. Baker (1987), Electric field and plasma density measurements in the strongly driven daytime equatorial electrojet: 1. The unstable layer and gradient drift waves, *J. Geophys. Res.*, *92*(A12), 13,578–13,596, doi:10.1029/JA092iA12p13578.

Ramkumar, T. K., S. Gurubaran, R. Rajaram, D. Tiwari, and K. S. Viswanathan (2010), A comparison study of zonal drift velocities measurements as seen by MF spaced antenna and HF Doppler radar in the Indian dip equatorial mesospheric and lower thermospheric (80–100 km) region, *J. Geophys. Res.*, *115*, A02306, doi:10.1029/2009JA014728.

Rastogi, R. G., and J. Mullen (1981), Intense daytime radio wave scintillations and sporadic *E* layer near the dip equator, *J. Geophys. Res.*, *86*(A1), 195–198, doi:10.1029/JA086iA01p00195.

Reddy, C. A., and C. V. Devasia (1977), VHF radar observations of gradient instabilities associated with blanketing E_s layers in the equatorial electrojet, *J. Geophys. Res.*, *82*(1), 125–128, doi:10.1029/JA082i001p00125.

Schmidt, M., and S. Peter Gary (1973), Density gradients and the Farley-Buneman instability, *J. Geophys. Res.*, *78*, 8261–8265, doi:10.1029/JA078i034p08261.

Shume, E. B., D. L. Hysell, and J. L. Chau (2005), Zonal wind velocity profiles in the equatorial electrojet derived from phase velocities of type II radar echoes, *J. Geophys. Res.*, *110*, A12308, doi:10.1029/2005JA011210.

Somayajulu, V. V., L. Cherian, K. Rajeev, G. Ramkumar, and C. Raghava Reddi (1993), Mean winds and tidal components during counter electrojet events, *Geophys. Res. Lett.*, *20*, 1443–1446, doi:10.1029/93GL00088.

Somayajulu, V. V., K. S. Viswanathan, K. S. V. Subbarao, and L. Cherian (1994a), Distortions in the height structure of the equatorial electrojet during counter electrojet events, *J. Atmos. Terr. Phys.*, *56*(1), 51–58, doi:10.1016/0021-9169(94)90175-9.

Somayajulu, V. V., R. Selvamurugan, C. V. Devasia, and L. Cherian (1994b), VHF backscatter radar observations of type I waves during a counter electrojet event, *Geophys. Res. Lett.*, *21*(18), 2047–2050, doi:10.1029/94GL01590.

Valladares, C. E., R. Sheehan, S. Basu, H. Kuenzler, and J. Espinoza (1996), The multi-instrumented studies of equatorial thermosphere aeronomy scintillation system: Climatology of zonal drifts, *J. Geophys. Res.*, *101*(A12), 26,839–26,850, doi:10.1029/96JA00183.

Vineeth, C., T. Pant, K. Kumar, L. Jose, S. Sumod, and S. Alex (2012), Counter equatorial electrojet: Analysis of the variability in daytime mesopause temperature and winds, *J. Atmos. Sol. Terr. Phys.*, *75-76*, 115–121, doi:10.1016/j.jastp.2011.07.005.

Wernik, A. W., C. H. Liu, and K. C. Yeh (1983), Modeling of spaced-receiver scintillation measurements, *Radio Sci.*, *18*(5), 743–764, doi:10.1029/RS018i005p00743.

Whitehead, J. D. (1961), The formation of the sporadic-*E* layer in the temperate zones, *J. Atmos. Terr. Phys.*, *20*, 49–58.

Yadav, V., B. Kakad, C. K. Nayak, G. Surve, and K. Emperumel (2014), Occurrence of blanketing E_s layer (E_{sb}) over the equatorial region during the peculiar minimum of solar cycle 24, *Ann. Geophys.*, *32*, 553–562, doi:10.5194/angeo-32-553-2014.

Yeh, K. C., and C. H. Liu (1982), Radio wave scintillations in the ionosphere, *Proc. IEEE*, *70*(4), 324–360, doi:10.1109/PROC.1982.12313.